Journal of ELECTRONIC MATERIALS, Vol. 46, No. 8, 2017
DOI: 10.1007/s11664-017-5473-1

Synthesis and Characterization of Polyol-Assisted Nano $Cu_{0.2}Ni_{0.2}Sn_{0.2}Ba_{0.4}$ Fe_2O_4 by a Wet Hydroxyl Route

S. PAVITHRADEVI,[1,7] N. SURIYANARAYANAN,[2] T. BOOBALAN,[3] S. VELUMANI,[4] M. CHANDRAMOHAN,[5] and M. MANIVEL RAJA[6]

1.—Park College of Engineering and Technology, Coimbatore, India. 2.—Department of Physics, Government College of Technology, Coimbatore, India. 3.—Department of Physics, PSG Polytechnic College, Coimbatore, India. 4.—Center for Research and Advanced Studies of the National Polytechnic Institute, Mexico City, Mexico. 5.—Vishnu Lakshmi College of Engineering and Technology, Coimbatore, India. 6.—Defence Metallurgical Research Laboratory, Ministry of Defence, Govt. of India, Hyderabad, India. 7.—e-mail: pavithradevi.naveen@gmail.com

Nanocrystalline spinel ferrite of composition $Cu_{0.2}Ni_{0.2}Sn_{0.2}Ba_{0.4}$ Fe_2O_4 has been synthesized by a wet hydroxyl chemical route in ethylene glycol as chelating agent and sodium hydroxide as precipitator at pH 8. Ethylene glycol has been used as the medium which serves as the solvent as well as a complexing agent. The synthesized particles are annealed at temperatures of 350°C, 700°C, and 1050°C. Thermogravimetric (TG) analysis confirms that at 240°C, ethylene glycol has evaporated completely, and a stable phase is formed above 670°C. Fourier transform infrared (FT-IR) spectroscopy of mixed $Cu_{0.2}Ni_{0.2}Sn_{0.2}Ba_{0.4}$ ferrite nanoparticles like as synthesized and annealed at 1050°C are recorded between 400 cm^{-1} and 4000 cm^{-1}. FT-IR appraises the structural formation of $Cu_{0.2}Ni_{0.2}Sn_{0.2}Ba_{0.4}$ Fe_2O_4 between the as-synthesized sample and the sample annealed at 1050°C. Structural characterizations of all the samples are carried out by x-ray diffraction (XRD) technique. XRD reveals that the particle size increases with the increase in annealing temperatures. Transmission electron microscopy (TEM) and scanning electron microscopy (SEM) confirms that the particles are flaky and spherical with the crystallite size in the range of 11–27 nm. The decrement of dielectric properties, like dielectric constant and dielectric loss, with the increment of frequency as seen in all the samples is an usual dielectric behavior of spinel ferrites. The lack of net magnetization is noticed immediately when the applied magnetic field is removed which prompts superparamagnetic behavior, as seen in all the samples.

Key words: X-ray diffraction, thermal analysis, FT-IR, dielectric properties, vibrational sample magnetometer

INTRODUCTION

The aim, combination and characterization of nanophase materials are the subject of current intense research. The study of numerous spinel-type ferrites is in terms of the synthesis of their nanoparticles at room temperatures by different methods, in terms of the potential applications of these nanosized magnetic materials in special technological areas, as well as to study the magnetic properties of the nanoferrite materials.[1–6] Nanosized ferrites with uniform and narrow particle size distribution are desirable for a variety of applications like targeted drug delivery, ferrofluids, medical imaging and other biomedical applications, magnetic data storage, etc.[7–11] Ferrite materials have strong ferromagnetic behavior and

(Received December 5, 2016; accepted March 21, 2017; published online March 28, 2017)

this behavior depends upon the electronic configuration of the atoms in the substances. Therefore, a good understanding of the electronic state of the elements presents in the ferrite structure is essential to describe its magnetic behavior.[12] Spinel ferrites have been extensively studied due to their fascinating properties like high resistivity, mechanical hardness, significant stability and promising memory storage capacity.[13–18] The properties of the nanosized ferrites are entirely different from those of their bulk counterparts in magnetic medium. Copper ferrites are very imperative for applications as well as for theoretical understanding of all spinel ferrites. The copper ferrite in powder form has been intensively studied in the past.[19] The high surface area of copper ferrite is prioritized for catalytic purposes. In general, high surface areas go along with small particle sizes. Hence, synthesis of nanosized copper ferrite particles will be worthwhile to study.[20] Nickel ferrite is a soft ferrite having low magnetic coercivity and high electrical resistivity. The high electrical resistivity and good magnetic properties make this ferrite an excellent core material for power transformers in electronics and telecommunication applications.[21] Barium ferrite is a famous permanent magnetic material due to its high coercivity and fairly large crystal anisotropy. However, it is also a leading candidate material for advanced magnetic recording media.[22] Nanoparticles with controlled sizes and properties can be synthesized by wet chemical techniques.[23–26]

EXPERIMENTAL TECHNIQUE

Sample Preparation

Nanocrystalline polyol-assisted $Cu_{0.2}Ni_{0.2}Sn_{0.2}Ba_{0.4}$ mixed ferrite is prepared by a wet hydroxyl chemical technique at pH 8. The chemicals used are high purity such as A.R. grade cupric chloride ($CuCl_2.2H_2O$), nickel chloride ($NiCl_2.6H_2O$), tin chloride ($SnCl_2.2H_2O$), barium chloride ($BaCl_2.2H_2O$), ferric chloride ($FeCl_3.2H_2O$), sodium hydroxide (NaOH), and ethylene glycol.

0.2 mol of cupric chloride, 0.2 mol of nickel chloride, 0.2 mol of tin chloride, 0.4 mol of barium chloride, and 2 mol of ferric chloride are weighed to a stoichiometric ratio and carefully dissolved into ethylene glycol as a chelating agent. Ethylene glycol helps in complex formation and acts as a capping agent. Then, the solution is mixed by constant stirring for 6 h. Then, the precipitate is obtained by adding NaOH solution drop-wise continuously till the pH reaches 8. The precipitate is washed several times with distilled water until it is free from impurities. The product is dried in a hot air oven at 120°C for 24 h, so that the water content evaporates and is eventually converted to black granules. This dried granule is powdered in an agate mortar after being cooled to room temperature.

Equipments Used for Characterization

The thermal analysis [thermogravimetry/differential thermal analysis (TG/DTA)] of the as-synthesized powder is done using a Perkin Elmer STA 6000. Synthesized polyol-assisted $Cu_{0.2}Ni_{0.2}Sn_{0.2}Ba_{0.4}$ ferrite samples are annealed at temperatures of 350°C, 700°C, and 1050°C for 2 h. Phase purity of the powder is confirmed by x-ray diffraction (XRD) studies using a PW3701 Philips diffractometer. The powder morphology is studied using a JEOL JEM model 2100 high-resolution transmission electron microscopy and SIGMA HV – Carl Zeiss With Bruker Quantax 200 field emission scanning electron microscopy. Selected powders are characterized for Fourier transform infrared spectroscopy (FT-IR) by SHIMADZU IRAffinity 1S. Sintered disc-shaped samples with silver electrodes are subjected to the measurements of dielectric constant and dielectric loss using a precision impedance analyzer (CJ6500B) at room temperature. Magnetic measurements like retentivity, coercivity, and saturation magnetization are performed using a vibrating sample magnetometer (VSM7407) at room temperature.

RESULTS AND DISCUSSION

Structural Analysis

Thermogravimetric Analysis (TGA) and Differential Thermal Analysis (DTA)

Thermogravimetric analysis (TGA) is a measure of mass loss (%) of a sample, as a function of increase in temperature. This method is used for determining the phase formation and studying the decomposition reaction present in the sample. TGA and DTA curves for polyol-assisted $Cu_{0.2}Ni_{0.2}Sn_{0.2}Ba_{0.4}$ ferrite is shown in Fig. 1. The sample is heated from room temperature to 1000°C at a rate of 10°C per minute in oxygen atmosphere. The first stage of weight loss is in a room-temperature range and followed by a faster loss which is completed at about 180°C. As per the curve, the first weight loss of around 11% is due to evaporation of water and removal of organic impurities, if any present, in the sample till 180°C. The DTA curve shows that this weight loss is accompanied by a sharp and intense endothermic peak around 100°C. The second and third weight loss occurs at the temperature range of 240°C and 670°C, respectively. This weight loss of around 7% is due to the dehydration of the O–H group in the spinel structure and some organic constituents such as ethylene glycol and decomposition of chlorides. The DTA curve shows two small exothermic peaks at 260°C and 280°C, while a strong and broad region from 650°C to 900°C show three exothermal peaks. Two of the exothermic peaks could be attributed to the evaporation of coordinated water, while the strong and broad region containing multi exothermic peaks could be due to the decomposition of the organic substance together with the evolution of great amounts of gases such as CO_2 and NO_x. The crystallization process appeared

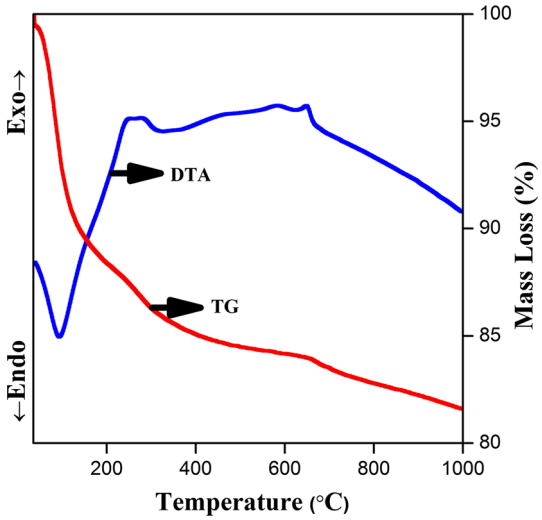

Fig. 1. TG and DTA curve of as-synthesized polyol-assisted $Cu_{0.2}Ni_{0.2}Sn_{0.2}Ba_{0.4}$ ferrite nanoparticles.

at 680°C. Above 700°C, no weight loss is observed; hence, the crystallization process was completed and pure ferrite could be observed. The net weight loss is found to be ~18%. At a higher decomposition temperature, the stronger bonding is created by the ferrite particles.[27]

X-ray Diffraction (XRD) Analysis

XRD patterns of polyol-assisted $Cu_{0.2}Ni_{0.2}Sn_{0.2}Ba_{0.4}$ ferrite samples annealed at 350°C, 700°C, and 1050°C for 2 h are shown in Fig. 2. As-synthesized samples annealed at 350°C exhibited an amorphous nature. No diffraction peaks are noticed which shows the lack of crystalline nature in the as-synthesized particles. This nature of these samples is also confirmed by high-resolution transmission electron microscopy (HR-TEM) on increasing annealing temperatures to 700°C and 1050°C. The XRD pattern consists of well-defined peaks, which confirms the single-phase nanoparticle nature of the prepared particles. The diffraction peaks corresponding to planes (1 1 1), (2 0 0), (4 2 0), (2 2 0), (2 2 3), (3 1 1), (2 2 2), (4 0 0), (3 3 1), (4 2 2), (5 1 1), (4 4 0) and (5 3 3) present a clear confirmation for the formation of single-phase cubic spinel ferrite. This data agrees with the standard Joint Committee on Powder Diffraction Standards (JCPDS) # (25-0283), # (74-1913), # (71-0693) and # (75-0427).

As the annealing temperature increases, the preferred orientation along the (3 1 1) plane also increases and a face-centered cubic spinel structure is obtained which has a space group of F, Fd_3m and a lattice constant of 8.2795 Å.[28,29] The average grain sizes of the samples are calculated using the Debye–Scherrer formula.

$$t = \frac{0.9\lambda}{\beta \cos\theta} \quad (1)$$

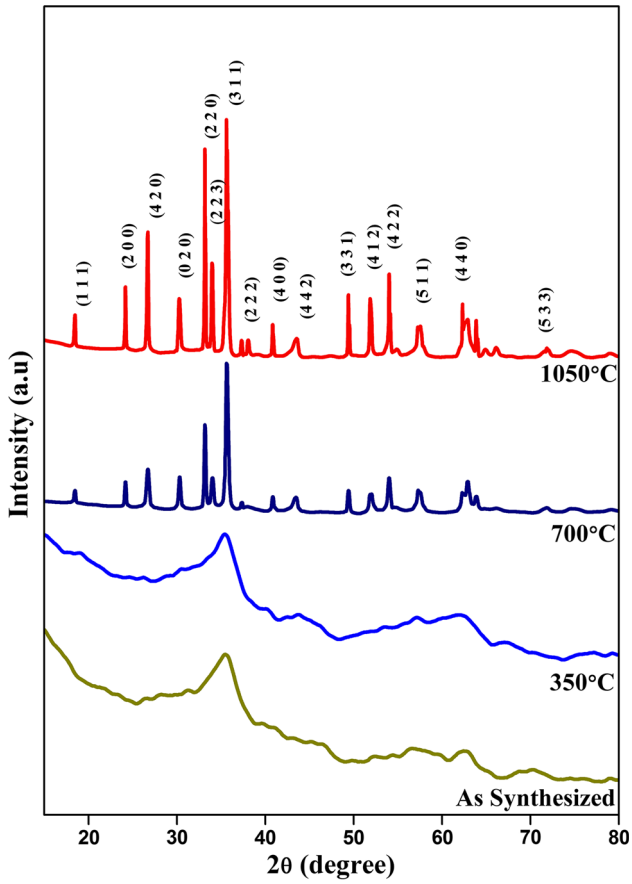

Fig. 2. XRD pattern of polyol-assisted $Cu_{0.2}Ni_{0.2}Sn_{0.2}Ba_{0.4}$.

where λ is the x-ray wavelength, θ is the Bragg's angle and β is the full width of the diffraction line at the half maximum intensity. The average crystallite size is found to be 19 nm. It is clearly seen that with an increase in annealing temperatures, all the peaks become sharper and this is an indication for the increase in the particle size. Thermal annealing induces coalescence of small grains by grain boundary diffusion which causes grain growth and, hence, the size of the nanoparticles increases.[30] In this system, ethylene glycol acts as the solvent, complexing agent as well as a capping molecule during the growth of the nuclei. It may form a complex with the metal ions through ethylene glycol intermediates which gives rise to the nano-sized particles.

Fourier Transform Infrared Spectroscopic (FT-IR) Analysis

The formation of polyol-assisted $Cu_{0.2}Ni_{0.2}Sn_{0.2}Ba_{0.4}$ ferrite of the as synthesized form and that annealed at 1050°C is supported by FT-IR spectra recorded between 400 cm^{-1} and 4000 cm^{-1}, as shown in Fig. 3. The ferrite can be considered as continuously bonded crystals, via ionic, covalent or Vander Waals forces, to the nearest neighbors. In ferrite, the metal ions can be situated in two different sublattices,

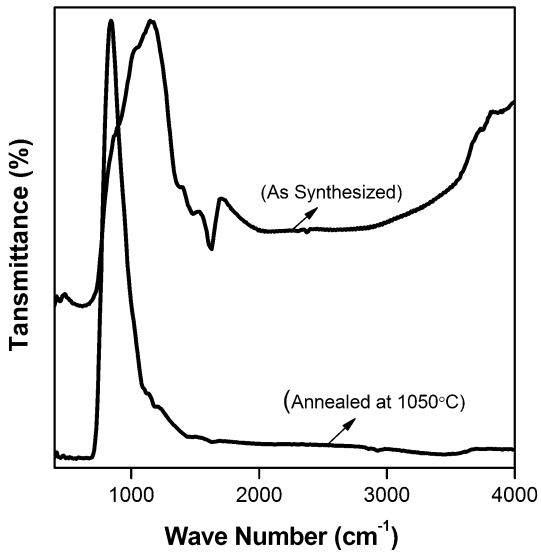

Fig. 3. FT-IR spectra of polyol-assisted $Cu_{0.2}Ni_{0.2}Sn_{0.2}Ba_{0.4}$ ferrite.

namely tetrahedral (A-sites) and octahedral (B-sites) according to the geometrical configuration of the nearest oxygen neighbor. The vibration spectra of spinel ferrites at the high-frequency band $\nu 1$ 600–500 cm^{-1} and the low-frequency band $\nu 2$ 440–400 cm^{-1} are attributed to the intrinsic vibration of the tetrahedral sites and the octahedral sites, respectively.[31] The absorption band around 1380–1640 cm^{-1} is due to the bending of the absorbed water molecules. The O–H stretching vibration interacting through H bonds is observed at 2376 cm^{-1}. Spectra consisting of ethylene glycol absorption bands at 1040 $cm^{-1,}$ 2878 cm^{-1}, and 2948 cm^{-1} are ascribed to C–OH stretching, symmetric (–CH2–), and asymmetric (–CH3–) vibrations.[32] When the sample is annealed at 1050°C, all the absorption bands disappear, except for metal oxide bands, which is clearly shown in Fig. 4. The IR absorption bands we observed below 1000 cm^{-1} can be attributed to the M–OH modes (M = Cu–Ni–Sn–Ba and Fe). The spectra indicates the existence of two absorption bands: $\nu 1$ at 550–570 cm^{-1} is caused by the stretching vibration of Fe^{3+}–O^{2-} in the tetrahedral metal–oxygen complexes and the absorption band $\nu 2$ at 401–486 cm^{-1} is caused by the metal–oxygen complexes in the octahedral sites. These bands are common features for all ferrites. It is also noticed that a very small peak at 2924 cm^{-1} is ascribed to the decomposition of water from ambient moisture. This is possibly due to sample handling to record the IR spectra, during which moisture was possibly adsorbed on the external surface of the particles.[33]

Morphological Analysis

High-Resolution Transmission Electron Microscopy (HR-TEM) Analysis

Figure 4a–d displays the as-synthesized polyol-assisted $Cu_{0.2}Ni_{0.2}Sn_{0.2}Ba_{0.4}$ ferrite nanoparticles and those annealed at 350°C, 700°C, and 1050°C, respectively. The distribution of these particles seems to be symmetric with the particle size in the range of 11–27 nm. Most of the particles appear spherical in shape; however, some elongated and flaky particles are also present, as shown in the TEM images. The magnetic interaction between the nanocrystallites and high surface energy of the nanoparticles renders them to be in agglomerated form. Agglomeration is implicit and it is linearly escalating with a rise in annealing temperatures. Hence, some degree of agglomeration appears inevitable. The agglomeration increases due to an inadequate amount of ethylene glycol as well as annealing temperature.[34]

Selected Area Electron Diffraction (SAED) Analysis

An SAED pattern of $Cu_{0.2}$ $Ni_{0.2}Sn_{0.2}Ba_{0.4}$ ferrite nanoparticles is shown in Fig. 4e. The diffuse intensity distribution in the SAED pattern verifies the nanocrystallinity of the material. The rings on the diffraction pattern are typical of a spinel $Cu_{0.2}Ni_{0.2}Sn_{0.2}Ba_{0.4}$ ferrite with nanostructure. The position and the relative intensities of the rings identified in the SAED pattern unambiguously confirm the cubic spinel structure.

Field Emission Scanning Electron Microscopy (FE-SEM) Analysis

SEM images of polyol-assisted $Cu_{0.2}Ni_{0.2}Sn_{0.2}Ba_{0.4}$ ferrite nanoparticles are shown in the Fig. 5a–d. The images display the spherical and sponge nature of the particles as well as slight agglomeration of the very fine particles due to interaction between magnetic nanoparticles.

Energy Dispersive x-ray Spectroscopy (EDS) Analysis

In order to confirm the chemical composition, EDS analysis is carried out and the typical data of the $Cu_{0.2}Ni_{0.2}Sn_{0.2}Ba_{0.4}$ ferrite nanoparticles is shown the Fig. 5e. In the present study, the compositional analysis obtained with this method could accurately quantify the Cu, Ni, Sn, Ba, and Fe contents within 2–3% error. It also confirms the absence of impurities in these samples. In this image, the presence of carbon is found due to the carbon grids used to hold the sample.

Dielectric Measurements

Dielectric Constant and Dielectric Loss

The variation of dielectric constant and dielectric loss as a function of frequency for the as-synthesized sample and those annealed at 350°C, 700°C, and 1050°C is shown in Fig. 6a and b. In our result, the value of dielectric properties like dielectric constant and dielectric loss decreases continuously with increasing frequency at room temperature. In most

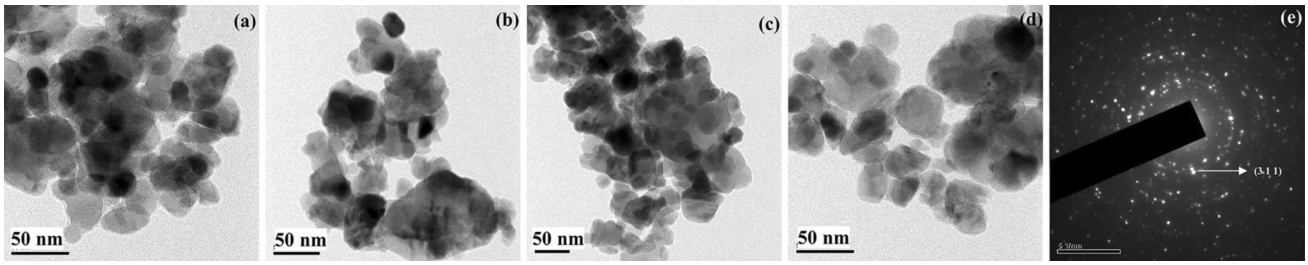

Fig. 4. HR-TEM image of polyol-assisted $Cu_{0.2}Ni_{0.2}Sn_{0.2}Ba_{0.4}$ ferrite nanoparticles. (a) As synthesized, (b) annealed at 350°C, (c) annealed at 700°C, (d) annealed at 1050°C, (e) selected area electron diffraction (SAED) pattern.

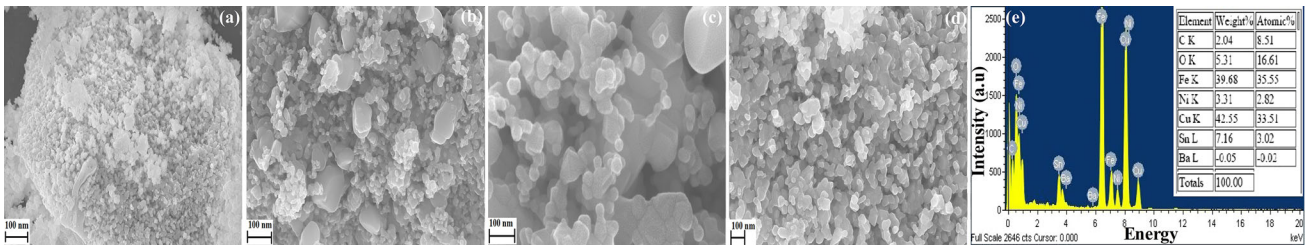

Fig. 5. FE-SEM image of polyol-assisted $Cu_{0.2}Ni_{0.2}Sn_{0.2}Ba_{0.4}$ ferrite nanoparticles. (a) As synthesized, (b) annealed at 350°C, (c) annealed at 700°C, (d) annealed at 1050°C, (e) energy dispersive x-ray spectroscopy (EDS).

of the ferrite samples, this normal behavior takes place.[35–37] According to Koop's phenomenological theory of solids, the solid consists of well-conducting grains and these grains are separated into weakly conducting grain boundaries.[38] The rapid fall of dielectric properties at lower frequencies and constant value at higher frequencies can be explained on the basis of space charge polarization and electronic polarization. The local displacement of the electrons in the direction of the applied field determines the polarization, which is due to the electronic exchange between Fe^{2+} and Fe^{3+} ions. Beyond a certain frequency range, these electrons contribute to the polarization. Therefore, the electric charge carriers cannot follow the alternating field and lag behind. Hence, the value of the dielectric constant decreases at the high-frequency region. The values of dielectric loss are high in the low-frequency region because more energy is required for electronic exchange.[39,40]

Magnetic Studies

Vibrating Sample Magnetometer (VSM) Analysis

Figure 7a dipicts the room-temperature hysteresis of polyol-assisted $Cu_{0.2}Ni_{0.2}Sn_{0.2}Ba_{0.4}$ ferrite nanoparticles. The magnetic data obtained is present in the Table I. Specific magnetization of all the samples is linear to the applied magnetic field and shows the superparamagnetic behavior. At the point when the measure of single domain particles additionally diminishes to the critical diameter, the coercivity approaches zero, and such particles become superparamagnetic. In a superparamagnetic state, the particles are sufficiently solid to suddenly demagnetize a formerly immersed gathering; in this manner, these particles have almost zero coercivity and have no hysteresis. A disordered solid exhibits a low value of saturation magnetization due to the prevention of core spins by surface spins, as observed in Fig. 7a.

Basically, the saturation magnetization of a spinel ferrite depends on its composition and particle size; at the same time, the coercive field also depends on composition, particle size and their shapes. The obtained result indicates the saturation magnetization increases with magnetic field and forms the single domain superparamagnetic particles.[41] The almost zero remanence and coercivity show the superparamagnetic behavior of nanoparticles.[42] The high value of saturation magnetization was attributed to the formation of a single phase of cubic $Cu_{0.2}Ni_{0.2}Sn_{0.2}$
$Ba_{0.4}$ ferrite phase with high crystallinity and fine crystallite size. Moreover, the variation of coercive field (Hc) with crystallite size can be explained on the basis of domain structure, critical diameter and the anisotropy of the crystal. A crystallite will instinctively break up into a number of domains in order to reduce the large magnetization energy in a single domain.[43] It is known that fine particles are easier to thermally activate to overcome the magnetic anisotropy.[44] As the sample is annealed at higher temperatures, the result indicates the grain growth; hence, this affects the particle size as well as ionic distribution.[45] The superparamagneticism with low

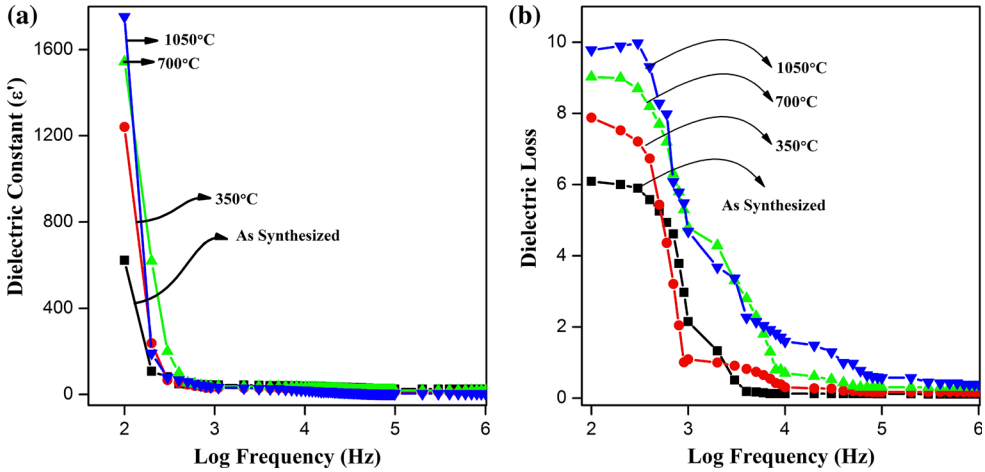

Fig. 6. (a,b) Dielectric constant and dielectric loss of polyol-assisted $Cu_{0.2}Ni_{0.2}Sn_{0.2}Ba_{0.4}$ ferrite nanoparticles.

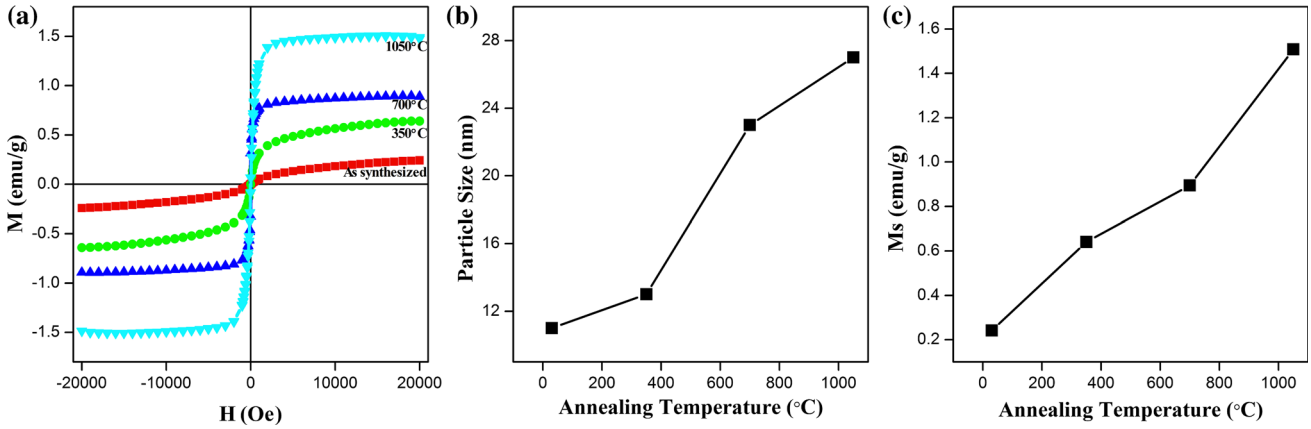

Fig. 7. (a, b, c) Hysteresis loop, plot between annealing temperature with particle size, and plot between annealing temperature with saturation magnetization of polyol-assisted $Cu_{0.2}Ni_{0.2}Sn_{0.2}Ba_{0.4}$ ferrite nanoparticles.

Table I. XRD and VSM parameters

Sample no.	Sample	Average particle size (nm)	Average coercive field Hc (Oe)	Average saturation magnetization (Ms, emu/g)	Average remanent magnetization (Mr, emu/g)
1	$Cu_{0.2}Ni_{0.2}Sn_{0.2}Ba_{0.4}$ [Fe_2O_4] As synthesized	11	11.31	0.24	0.0010
2	$Cu_{0.2}Ni_{0.2}Sn_{0.2}Ba_{0.4}$ [Fe_2O_4] Annealed at 350°C	13	11.34	0.64	0.0011
3	$Cu_{0.2}Ni_{0.2}Sn_{0.2}Ba_{0.4}$ [Fe_2O_4] Annealed at 700°C	23	11.50	0.89	0.0211
4	$Cu_{0.2}Ni_{0.2}Sn_{0.2}Ba_{0.4}$ [Fe_2O_4] Annealed at 1050°C	27	20.77	1.51	0.0752

value of coercive field allows the material to magnetize and demagnetize easily with a small magnetic loss.[46] The linear variation of the particle size and saturation magnetization is a function of the annealing temperature, as shown in Fig. 7b and c.

CONCLUSION

A simple and economic co-precipitation method has been used for the synthesis of nanosized polyol-assisted $Cu_{0.2}Ni_{0.2}Sn_{0.2}Ba_{0.4}$ ferrites. TGA and DTA curves show that the stable phase formation and

crystallinity starts at 680°C. The FT-IR spectra confirmed the $Cu_{0.2}Ni_{0.2}Sn_{0.2}Ba_{0.4}$ ferrite's formation. XRD patterns reveal the single-phase cubic spinel compound has an average crystallite size of 19 nm. The particle size of the samples increased with annealing temperature. TEM revealed the crystallite size between 11 nm and 27 nm, and SAED patterns authenticated the crystallinity. SEM, and EDX analysis confirm the particle size and chemical composition, respectively. The value of dielectric constant and dielectric loss decreases continuously with increase in the frequency at room temperature. The magnetic properties of the ferrite samples are strongly affected by the annealing temperatures. From VSM analysis, specific magnetizations of all the samples are linear and exhibit a soft and superparamagnetic behavior.

REFERENCES

1. K. Dyal, M. Loos, S.W. Noto, C. Chang, K.V.P.M. Spagnoli, A. Shafi, M. Ulman, and R.A.Gross Cowman, *J. Am. Chem. Soc.* 125, 1684 (2003).
2. E.J. Choi, Y. Ahn, S. Kim, D.H. An, K.U. Kang, B.G. Lee, K.S. Baek, and H.N. Oak, *J. Magn. Magn. Mater.* 262, L198 (2003).
3. S. Sinha, G.V.S. Nayar, P.A. Murthy, V. Joy, and P. Ramachandrarao Rao, *J. Mater. Res.* 18, 1309 (2003).
4. C. Caizer and M. Stefaneson, *J. Phys. D Appl. Phys.* 35, 3035 (2002).
5. I. Hrianca, C. Caizer, and Z. Schlett, *J. Appl. Phys.* 92, 2125 (2002).
6. C. Liu, B. Zou, A.J. Rondinone, and Z.J. Zhang, *J. Am. Chem. Soc.* 122, 6263 (2000).
7. M. Shinkai, *J. Biosci. Bioeng.* 94, 606 (2002).
8. A.S. Lubbe, C. Alexiou, and C. Bergemann, *J. Surg. Res.* 95, 200 (2001).
9. L.X. Tiefenauer, A. Tschirky, G. Kuhne, and R.Y. Andres, *J. Magn. Res. Imaging* 14, 391 (1996).
10. R. Skmoski, *J. Phys. Condens. Matter* 15, R841 (2003).
11. M.R.J. Gibbs, *Curr. Opin. Solid State Mater. Sci.* 7, 83 (2003).
12. M. Srivastava, A.K. Ojha, S. Chaubey, and A. Materny, *J. Alloys Compd.* 481, 515 (2009).
13. S. Prasad and N.S. Gajbhiye, *J. Alloys. Compd.* 265, 87 (1998).
14. K.V.P.M. Shaff, Y. Koltypin, and A. Gedaken, *J. Phys. Chem. B* 101, 6409 (1997).
15. A. Kau, S. Gubbala, and R.D.K. Misra, *J. Magn. Magn. Mater.* 277, 350 (2004).
16. P.P. Hankare, V.T. Vader, N.M. Patil, S.D. Jadhav, U.B. Sankpal, M.R. Kadam, B.K. Chougule, and N.S. Gajbhiye, *J. Mater. Chem. Phys.* 113, 233 (2009).
17. S. Gin, S. Samanta, S. Maji, and S. Gangli, *J. Magn. Magn. Mater.* 288, 296 (2005).
18. G.R. Dube and V.S. Darshane, *J. Mol. Catal.* 79, 285 (1993).
19. S. Tao, F. Gao, X. Liu, and O.T. Sorensen, *J. Mater. Sci. Eng. B* 77, 172 (2000).
20. W. Lv, B. Liu, Z. Luo, X. Ren, and P. Zhang, *J. Alloys Compd.* 465, 261 (2008).
21. T. Abraham, *J. Am. Ceram. Soc. Bull.* 73, 62 (1994).
22. M.P. Sharrock and L.W. Carlson, *IEEE Trans. Magn.* 31, 2871 (1995).
23. A.S. Albuquerque, J.D. Ardisson, and W.A.A. Macedo, *J. Appl. Phys.* 87, 4352 (2000).
24. A. Dias, R.L. Moreira, and N.D.S. Mohallem, *J. Phys. Chem. Solids* 58, 543 (1997).
25. C.S. Kim, Y.S. Yi, and K.T.P. Park, *J. Appl. Phys.* 85, 5223 (1999).
26. L. Yu, S. Cao, Y. Liu, J. Wang, C. Jing, and J. Zhang, *J. Magn. Magn. Mater.* 301, 100–106 (2006).
27. M.S. Hegde, D. Larcher, L. Dupont, B. Beaudoin, K. Tekaia-Elhsissen, and J.M. Tarascon, *Solid State Ion.* 93, 33 (1997).
28. J.C. Waerenborgh, M.O. Figueiredo, J.M.P. Cabral, and L.C.J. Pereira, *J. Solid State Chem.* 111, 300 (1994).
29. J.A. Toledo-Antonio, N. Nava, M. Martinez, and X. Bokhimi, *J. Appl. Catal. A Gen.* 234, 137 (2002).
30. J. Sengupta, R.K. Sahoob, K.K. Bardhana, and C.D. Mukherjee, *J. Mater. Lett.* 65, 2572 (2011).
31. L. Li, J. Jiang, and F. Xu, *J. EurPolym.* 42, 2221 (2006).
32. S. Thimmaiah, M. Rajamathi, N. Singh, P. Bera, F. Meldrum, N. Chandrasekhar, and R. Seshadri, *J. Mater. Chem.* 11, 3215 (2001).
33. S Farhadi and N Rashidi, *J. Polyhedron.* 29, 2959 (2010).
34. J. Giri, T. Sriharsha, and D. Bahadur, *J. Mater. Chem.* 14, 875 (2004).
35. D. Ravinder, G.R. Mohan, N. Prankishan, and D.R. Sagar, *J. Mater. Lett.* 44, 256 (2000).
36. H. Ismael, M.K. ElNimr, A.M. Abou El Ata, M.A. El Hiti, M.A. Ahmed, and A.A. Murakhowskii, *J. Magn. Magn. Mater.* 150, 403 (1995).
37. M.A. El Hiti, M.A. Ahmed, M.M. Mosaad, and S.M. Attia, *J. Magn. Magn. Mater.* 150, 399 (1995).
38. C.G. Koops, *J. Phys. Rev.* 83, 121 (1951).
39. T. Boobalan, N. Suriyanarayanan, and S. Pavithradevi, *J. Mater. Sci. Semicond. Process.* 16, 1695 (2013).
40. M.J. Iqbal, N. Yaqub, B. Sepiol, and B. Ismail, *J. Mater. Res. Bull.* 46, 1837 (2011).
41. J.C. Aphesteguy, S.E. Jacobo, N.N. Schegoleva, and G.V. Kurlyandskaya, *J. Alloys Compd.* 495, 509 (2010).
42. M. Jalaly, M.H. Enayati, and F. Karimzadeh, *J. Alloys Compd.* 480, 737 (2009).
43. M.A. Gabal, *J. Mater. Lett.* 64, 1887 (2010).
44. X. Cao and L. Gu, *J. Nanotechnol.* 16, 180 (2005).
45. J.P. Chen, C.M. Sorensen, K.J. Klabunde, G.C. Hadjipanayis, E. Devlin, and A. Kostikas, *J. Phys. Rev. B.* 54, 9288 (1996).
46. S. Deka and P.A. Joy, *J. Mater. Chem. Phys.* 100, 98 (2006).